$6p_{1/2,3/2}nf\ J=1-5$ autoionizing series of barium

M. Abutaleb,* R. J. de Graaff, W. Ubachs, and W. Hogervorst
Laser Centre Free University Amsterdam, Fakulteit Natuurkunde en Sterrenkunde, De Boelelaan 1081, 1081 HV Amsterdam, The Netherlands
(Received 8 March 1991)

The $6pnf$ series of barium converging to both $6p_{1/2}$ and $6p_{3/2}$ limits were investigated in a two-step pulsed-laser experiment. From $6s5d\ ^3D_{1,2,3}$ metastable atoms, discharge populated in an atomic beam, 11 out of the full manifold of 12 autoionizing $6p_{1/2,3/2}nf\ J=1$–5 Rydberg series were excited via selected $5d6p\ J=0$–4 doubly excited intermediate states. For each value of the total angular momentum J, the data were analyzed using R-shifted multichannel-quantum-defect theory. The autoionization rates of the different series compare well with a model for autoionization based upon only a direct Coulomb interaction mechanism with neglect of exchange effects. The multiplet level structure of the $6pnf$ configuration for a particular n Rydberg manifold was analyzed in terms of Slater integrals. The level ordering of $6pnf\ J$ substates could only be explained by including a large exchange parameter. Some $6pnp$ series were also observed, in particular $6p_{3/2}np_{3/2}\ J=3$.

PACS number(s): 32.80.Dz, 32.30.−r

I. INTRODUCTION

Barium continues to be an attractive atom to study the effects of interactions of two valence electrons. This is due to the low energy of doubly excited states, which are readily excited with pulsed lasers in the visible and ultraviolet part of the spectrum. The doubly excited $6pnl$ autoionizing Rydberg states have especially attracted attention. The classical vacuum-ultraviolet one-photon absorption studies from the $6s^2\ ^1S_0$ ground state [1,2] are well known, but were restricted to $J=1$ odd-parity states of $6pns$ and $6pnd$ configurations. Detailed studies of $6pnl,J$ states of different parities and angular momenta became feasible using laser-spectroscopic techniques. In particular, isolated-core-excitation (ICE) experiments have been quite successful. In the ICE scheme a bound $6snl$ Rydberg state is prepared by absorption of one or more photons, followed by excitation of the strong ionic $6s$-$6p$ transition of the core electron. In recent years studies of $6pns$ [3], $6pnp$ [4–6], $6pnd$ [7–10], $6png$ [11], $6pnh$ [12], and even of high-angular-momentum circular states $6pnl$ $(l=n-1)$ for n up to 13 [13] were reported. Several $6pnf$ autoionizing series were studied by Bente and Hogervorst [12] and by Jones, Dai, and Gallagher [14], but analyses were somewhat hampered because of perturbations in the $6snf$ intermediate bound Rydberg states.

In this article observations on 11 out of the manifold of 12 $6pnf$ autoionizing Rydberg series converging to the $6p_{1/2}$ (four series) and the $6p_{3/2}$ limit (eight series) will be presented. Experimentally a two-step laser-excitation scheme was used, in which a first laser transfers population from $6s5d\ ^3D_{1,2,3}$ metastable states to $J=0$–4 states of the $5d6p$ configuration. The metastable states were produced in a discharge maintained in an atomic beam. After the preparation of intermediate doubly excited states, a second (uv) laser excited the $6pnf$ Rydberg series with J values of 1–5. This scheme has the practical advantage that it allows for the excitation of a complete Rydberg series in a continuous wavelength scan, whereas in the ICE scheme for each individual value of the principal quantum number n a spectrum has to be recorded. Main advantages of the current scheme are that channel interactions show at first sight in the recorded features [4] and that the oscillator strength distribution from a theoretical model can be tested for consistency by comparing with the observed intensities over a wide range of n values.

The wealth of data on the 11 observed $6pnf$ series was analyzed in two complementary ways. Channel interactions, such as between $6p_{3/2}nf$ and $6p_{1/2}nf$ configurations only occur between series with the same J value and are treated in the R-shifted matrix formalism of multichannel-quantum-defect theory (MQDT) [15]. The most complicated case is that of $J=3$ with four bound channels, two converging to the $6p_{3/2}$ and two to the $6p_{1/2}$ limit, mutually interacting as well as with several underlying continua. Secondly the 11 states belonging to a certain n value are treated as a fine-structure multiplet and their level energies are analyzed in terms of spin-orbit and Slater direct and exchange electrostatic interactions. Apart from the recent analysis of the multiplet level structure of the $6pnp$ manifold by Carre *et al.* [6], no such procedure has been undertaken for a large and almost complete manifold of autoionizing $6pnl$ states.

In recent years theoretical models for the calculation of autoionization rates were developed by Nikitin and Ostrovsky [16] and by Poirier [17]. These models were based upon the assumption that for large $l(l\geq 3)$ the autoionization rates are determined solely by the direct electrostatic long-range interaction between the two valence electrons. While the calculations matched observations of autoionization rates of $6png$ [11] quite well, they are not suited for an explanation of ultranarrow $6pnp\ J=1$ autoionization resonances recently reported by de Graaff *et al.* [4]. Obviously for $l<3$, short-range

interactions, such as exchange effects, influence the autoionization rates of $6pnl$ Rydberg states. The interest of the present study therefore lies in the investigation of the autoionization mechanism for the $l=3$ case. As will be shown, the direct long-range Coulomb interaction also dominates the autoionization process for $l=3$. In previous studies rates of autoionization were studied as a function of the orbital angular-momentum quantum number l of the Rydberg electron [13]. The availability of data within a fine-structure multiplet of one electronic configuration allows for an investigation of the dependence of autoionization rates on the angular-momentum coupling of the two electrons.

The paper is organized as follows. After a description of the experimental setup in Sec. II, the observations on $6pnf$ will be presented for each particular J separately in Sec. III, where channel mixing is analyzed in the phase-shifted R'-matrix formalism. Observations on $6pnp$ $J=3$ features are also included. In Sec. IV a Slater-Condon analysis of the fine-structure energy level spacings within the $6pnf$ multiplet is presented. Section V focuses on the autoionization rates and a comparison with the calculations from first principles by Poirier [17,18]. Finally in Sec. VI some concluding remarks are made.

II. EXPERIMENTAL PROCEDURE

The experimental setup is the same as described in a previous report on interacting $6p_{1/2,3/2}np$ and $6p_{3/2}nf$ $J=1$ autoionizing series in barium [4]. With a low-voltage discharge in front of an oven orifice a small fraction of barium atoms in the resulting beam was transferred to metastable $6s5d\ ^3D_{1,2,3}$ states. A first dye laser, pumped by the 532-nm second-harmonic output of a Nd:YAG laser (Quanta-Ray GCR-4) and operating on rhodamine 640, DCM (4-dicyanomethylene-2-methyl-6-(*p*-dimethylaminostyrl)-4 1-1-pyran), and pyridine dyes to cover the wavelength range 600–767 nm, was tuned onto one of the well-known $6s5d$-$5d6p$ transitions [19]. The power of the first laser was set to saturate the specific $6s5d$-$5d6p$ transition. With the assumption of an equal population density within the $6s5d\ ^3D_{1,2,3}$ multiplet (about 1% each) the number of prepared atoms in the different $5d6p$ multiplet states then is a constant. A level scheme including energies of the $6s5d$ and $5d6p$ levels and transition wavelengths is shown in Fig. 1.

A second tunable uv laser, spatially and temporarily overlapping the first laser in the interaction zone with the atomic beam, was then tuned in the range 239–289 nm to further excite barium into $6p_{1/2}nf$ and $6p_{3/2}nf$ autoionizing states. This broad uv tuning range was necessary to cover all transitions from the $5d6p$ intermediate levels used to excite the autoionizing states. uv radiation in the range $\lambda>267$ nm was produced by 532-nm pumping of red dyes and subsequent frequency doubling in potassium dihydrogen phosphate, while the range $\lambda<267$ nm was covered by Nd:YAG third-harmonic pumping of coumarine dyes and doubling in a β–barium borate crystal. The bandwidth of the uv laser was 0.45 cm^{-1}. The $6pnf$ series were excited with a uv laser power of 1 mJ/pulse.

The $6pnf$ autoionizing resonances were monitored by detection of photoelectrons with an electron multiplier.

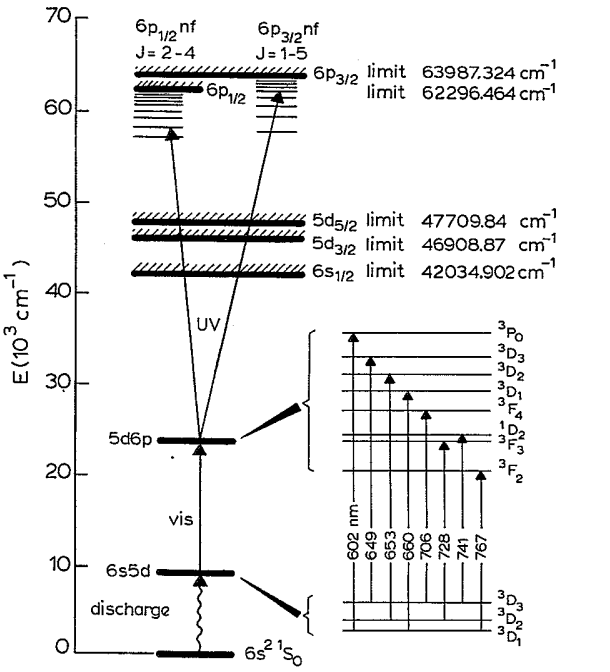

FIG. 1. Energy-level diagram showing the different excitation schemes in the two-color laser experiment. The fine-structure splittings of the $6s5d$ and $5d6p$ configuration are not drawn to scale.

In between the field-free interaction zone and the detector, a small repulsive voltage was applied, selecting photoelectrons with translational energies larger than 2 eV. Suppression of the contribution of slow electrons turned out to be necessary to eliminate a large signal background caused by direct nonresonant photoionization of $6s5d$ metastable barium atoms by uv radiation. Secondly, to reduce residual uv-induced background the visible laser beam was interrupted at half the repetition frequency of the pump laser and signal intensities of alternate laser shots were subtracted (by computer). Signal averaging was applied to 12 shots per wavelength setting.

An important consequence of the suppression of slow electrons was that one autoionization channel could not be observed. $6p_{3/2}nf$ states above the $6p_{1/2}$ limit autoionize into a barium ion in the $6s_{1/2}$, $5d_{3/2}$, $5d_{5/2}$, or $6p_{1/2}$ state. Autoionization into the $6p_{1/2}\epsilon l$ channel produces slow electrons, which were not detected in the chosen setup. Consequently the recorded signal intensities of $6p_{3/2}nf$ resonances did not immediately reflect the number of excited atoms. As the coupling to $6p_{1/2}\epsilon l$ autoionization channels may be different for each $6p_{3/2}nf$ J state, the fraction of neglected signal might depend on the particular series under investigation. The signal intensities of $6p_{1/2}nf$ resonances and $6p_{3/2}nf$ states below the $6p_{1/2}$-ion limit (at 62 296.464 cm^{-1}) were not affected, as they only decay into $5d\epsilon l$ and $6s\epsilon l$ channels producing fast electrons. Additionally the suppression grid induces an energy dependence in the response of the detection system. As the electron energy of an autoionization process into $6s\epsilon l$ channels is 0.5 eV higher than for the pro-

cesses into $5d\epsilon l$ channel, the former process will be favored in the detection. Finally the instrumental effect of varying laser beam overlap on the observed intensities should be mentioned, which becomes apparent in long-wavelength scans.

The energy positions of the $6pnf$ resonances were calibrated by measuring the wavelengths of the visible output of the second tunable dye laser in a home-built echelle-grating wavelength meter (accuracy 0.2 cm^{-1}) and adding the energies of the known $5d6p$ intermediate resonances. uv-induced $6s^2$-$6snp$ $J=1$ resonances, visible in the second (background) signal channel were used as well for calibration. The accuracy in the energy determination of the narrowest $6pnf$ resonances was about 0.3 cm^{-1}, while the accuracy for broad features at low n is estimated at 10% of the resonance width.

III. MEASUREMENTS AND INTERPRETATION; MQDT ANALYSES

The two-electron configuration $6pnf$ gives rise to 12 fine-structure states and so to 12 Rydberg series. One $J=1$, a $J=5$, and two $J=2$, 3, and 4 $6p_{3/2}nf$ series converge to the $6p_{3/2}$-ion limit. The angular momenta of $6p_{1/2}nf$ couple to one $J=2$, a $J=4$, and two $J=3$ series converging to the $6p_{1/2}$ limit. In general Rydberg series, or channels, with a common total angular momentum J exhibit interaction and will be dealt with together. From the prepared fine-structure states of the $5d6p$ multiplet, of which $^3P_0$ (25 642.103 cm^{-1}), $^3D_3$ (24 979.810 cm^{-1}), $^3D_2$ (24 531.490 cm^{-1}), $^3D_1$ (24 192.011 cm^{-1}), $^3F_4$ (23 757.029 cm^{-1}), $^1D_2$ (23 074.416 cm^{-1}), $^3F_3$ (22 947.402 cm^{-1}), and $^3F_2$ (22 064.623 cm^{-1}) were used, $6pnf$ Rydberg series were recorded as a function of the wavelength of the uv laser. Before discussing details of the observations and channel interactions for each value of J separately, some general remarks will be made.

The general selection rule for a $5d6p\,J$–$6pnf\,J'$ transition is $\Delta J=0,\pm1$, and therefore several series might be excited from a chosen $5d6p$ intermediate substrate. The oscillator strengths of $5d6p$-$6pnf$ transitions could be calculated assuming jk coupling for the $6pnf$ configuration and taking the wave-function composition of the $5d6p$ wave functions on an LS basis as determined by Grundevik *et al.* [19]. In Table I the results of these oscillator strength calculations are listed for transitions involving all $5d6p$ intermediate substates used and all possible $6p_{1/2,3/2}nf[k]\,J$ final states. It is obvious that $\Delta J=-1$ transitions are very weak and may be neglected. Furthermore, in all cases a $\Delta J=+1$ transition is the strongest. Depending on the particular intermediate state another $\Delta J=+1$ or a $\Delta J=0$ transition is second in line strength. The actual wave functions of the $6pnf$ series are linear combinations of the jk basis functions. The mixing coefficients depend on the values of fine-structure parameters to be determined in this study. In the calculation of line strengths for an *a posteriori* comparison with observations these mixing coefficients should be taken into account.

In the present study we aimed at a self-consistent method for the correct assignment of the observed spectral features in terms of angular-momentum quantum numbers. An initial assignment was made using jk-coupled wave functions and the corresponding oscillator strengths given in Table I. In cases where two $6pnf\,J$ states were excited the (asymmetric) shapes of observed resonances were inspected for a decision to treat the observed features as, e.g., a single or a double series converging to the same limit. From such a first tentative assignment a multiplet structure with estimated fine-structure parameters for the $6pnf$ manifold is derived. These fine-structure parameters in turn determine the wave-function composition [20], and a calculation of line strengths based upon these mixed wave functions was performed next. After reassignment, if necessary, this procedure may be repeated until a consistent framework of assignments and line strengths results.

A comparison of observed and calculated intensities bears some risk as the observed intensity of $6p_{3/2}nf$ states does not fully represent the number of excited atoms but rather the fraction that autoionizes into the $5d$ and $6s$ continua, thereby producing fast electrons. However, it will be shown later that due to the relatively small branching ratio for ionization into the $6p_{1/2}\epsilon l$ continuum ($<25\%$) this is a minor effect. The observed intensities in excitation of $6p_{1/2}nf$ states are not affected by unobserved ionization channels.

In a first tentative analysis the energies and quantum defects of the $6p_{3/2}nf\,J$ resonances were determined. The quantum defects were derived from positions of either single-peak or double-peak Lorentzian fits to the excitation profiles. For the $6p_{3/2}nf\,J=1$ and 5 series the quantum defects follow from an analysis of single-peak resonances. The $6p_{3/2}nf\,J=4$ spectrum allowed for an unambiguous double-peak analysis. For $6p_{3/2}nf\,J=3$ the quantum defect of one series ($\delta=0.34$) could be determined from a single Lorentzian peak analysis on the observed $5d6p\,^1D_2$–$6pnf$ $J=3$ spectrum. The $5d6p\,^3D_2$–$6p_{3/2}nf\,J$ spectrum was analyzed with double peaks, with a second $J=3$ series appearing at a quantum defect of $\delta=0.23$. Of the two existing $6p_{3/2}nf\,J=2$ channels only one was observed. The spectrum of $5d6p\,^3D_1$–$6p_{3/2}nf\,J$ was fitted to single Lorentzian peaks, as no asymmetries appeared in the observed features. The quantum defects of all four $6p_{1/2}nf$ series were obtained from single-peak fittings to the observed spectral lines. The two $6p_{1/2}nf\,J=3$ series appeared as single peaks in different excitation schemes, using $^1D_2$ and $^3D_2$ for one series and $^3F_2$ for the other. The large amount of experimental data does not encourage a presentation of all line positions in tables.

In order to verify a preliminary assignment of fine-structure levels also the direct electrostatic quadrupole interaction was calculated, the result of which was presented in part by Bente and Hogervorst [12]. The angular dependence of the matrix elements for this interaction

$$W_Q^{\text{geom}}=\langle 6p_{3/2}nf\;J|C_1^{(2)}C_2^{(2)}|6p_{3/2}nf\;J\rangle \qquad (1)$$

gives the relative splittings between fine-structure components. With jk-coupled wave functions for $6p_{3/2}nf$

TABLE I. Calculated oscillator strengths for transitions between $5d6p$-$6pnf$ multiplet states. For $5d6p$ the wave-function composition of Grundevik *et al.* [19] was taken. In the first column the line strengths in transitions to jk-coupled $6pnf$ states are listed (starting point of the analysis in Sec. III), while in the last column the line strengths are given for transitions to $6pnf$ states with the wave function composition as determined in the fine-structure analysis of Sec. IV.

Initial state	Final state	Intensity [j,k]	Intensity Mixed wave functions
$5d6p\ ^3P_0$	$6p_{3/2}nf\ [k=3/2]\ J=1$	0.2000	0.2000
$5d6p\ ^3D_1$	$6p_{1/2}nf\ [k=5/2]\ J=2$	0.3120	0.3142
	$6p_{3/2}nf\ [k=3/2]\ J=1$	0.0734	0.0734
	$6p_{3/2}nf\ [k=3/2]\ J=2$	0.0017	0.0003
	$6p_{3/2}nf\ [k=5/2]\ J=2$	0.2129	0.2119
$5d6p\ ^1D_2$	$6p_{1/2}nf\ [k=5/2]\ J=2$	0.0079	0.0077
	$6p_{1/2}nf\ [k=5/2]\ J=3$	0.2240	0.2443
	$6p_{1/2}nf\ [k=7/2]\ J=3$	0.0267	0.0084
	$6p_{3/2}nf\ [k=3/2]\ J=1$	0.0010	0.0010
	$6p_{3/2}nf\ [k=3/2]\ J=2$	0.0235	0.0274
	$6p_{3/2}nf\ [k=5/2]\ J=2$	0.0651	0.0614
	$6p_{3/2}nf\ [k=5/2]\ J=3$	0.1213	0.0259
	$6p_{3/2}nf\ [k=7/2]\ J=3$	0.5305	0.6234
$5d6p\ ^3D_2$	$6p_{1/2}nf\ [k=5/2]\ J=2$	0.0010	0.0011
	$6p_{1/2}nf\ [k=5/2]\ J=3$	0.1717	0.2134
	$6p_{1/2}nf\ [k=7/2]\ J=3$	0.1190	0.0792
	$6p_{3/2}nf\ [k=3/2]\ J=1$	0.0199	0.0199
	$6p_{3/2}nf\ [k=3/2]\ J=2$	0.0633	0.0545
	$6p_{3/2}nf\ [k=5/2]\ J=2$	0.1367	0.1454
	$6p_{3/2}nf\ [k=5/2]\ J=3$	0.2377	0.3501
	$6p_{3/2}nf\ [k=7/2]\ J=3$	0.2508	0.1365
$5d6p\ ^3F_2$	$6p_{1/2}nf\ [k=5/2]\ J=2$	0.0751	0.0753
	$6p_{1/2}nf\ [k=5/2]\ J=3$	0.0630	0.0144
	$6p_{1/2}nf\ [k=7/2]\ J=3$	0.7994	0.8489
	$6p_{3/2}nf\ [k=5/2]\ J=1$	0.0017	0.0017
	$6p_{3/2}nf\ [k=5/2]\ J=2$	0.0047	0.0086
	$6p_{3/2}nf\ [k=7/2]\ J=2$	0.0124	0.0084
	$6p_{3/2}nf\ [k=5/2]\ J=3$	0.0431	0.0422
	$6p_{3/2}nf\ [k=7/2]\ J=3$	0.0000	0.0009
$5d6p\ ^3D_3$	$6p_{1/2}nf\ [k=5/2]\ J=2$	0.0012	0.0012
	$6p_{1/2}nf\ [k=5/2]\ J=3$	0.0183	0.0183
	$6p_{1/2}nf\ [k=7/2]\ J=3$	0.0252	0.0252
	$6p_{1/2}nf\ [k=7/2]\ J=4$	0.5114	0.5115
	$6p_{3/2}nf\ [k=3/2]\ J=2$	0.0055	0.0071
	$6p_{3/2}nf\ [k=5/2]\ J=2$	0.0108	0.0092
	$6p_{3/2}nf\ [k=5/2]\ J=3$	0.1720	0.1646
	$6p_{3/2}nf\ [k=7/2]\ J=3$	0.0026	0.0099
	$6p_{3/2}nf\ [k=7/2]\ J=4$	0.6414	0.6148
	$6p_{3/2}nf\ [k=9/2]\ J=4$	0.0115	0.0380
$5d6p\ ^3F_3$	$6p_{1/2}nf\ [k=5/2]\ J=2$	0.0012	0.0013
	$6p_{1/2}nf\ [k=5/2]\ J=3$	0.0245	0.0185
	$6p_{1/2}nf\ [k=7/2]\ J=3$	0.0184	0.0245
	$6p_{1/2}nf\ [k=7/2]\ J=4$	0.4955	0.4989
	$6p_{3/2}nf\ [k=3/2]\ J=2$	0.0023	0.0019
	$6p_{3/2}nf\ [k=5/2]\ J=2$	0.0099	0.0103
	$6p_{3/2}nf\ [k=5/2]\ J=3$	0.0356	0.0686
	$6p_{3/2}nf\ [k=7/2]\ J=3$	0.1093	0.0763
	$6p_{3/2}nf\ [k=7/2]\ J=4$	0.1525	0.4167
	$6p_{3/2}nf\ [k=9/2]\ J=4$	0.5508	0.2829
$5d6p\ ^3F_4$	$6p_{1/2}nf\ [k=5/2]\ J=3$	0.0000	0.0000
	$6p_{1/2}nf\ [k=7/2]\ J=3$	0.0000	0.0000
	$6p_{1/2}nf\ [k=7/2]\ J=4$	0.0000	0.0000
	$6p_{3/2}nf\ [k=5/2]\ J=3$	0.0092	0.0121
	$6p_{3/2}nf\ [k=7/2]\ J=3$	0.0051	0.0021
	$6p_{3/2}nf\ [k=7/2]\ J=4$	0.1786	0.2141
	$6p_{3/2}nf\ [k=9/2]\ J=4$	0.0357	0.0002
	$6p_{3/2}nf\ [k=9/2]\ J=5$	1.5714	1.5714

states nearly equidistant ordering in four k states results starting from highest energy (smallest quantum defect): $6p_{3/2}nf$ $[k=3/2]$, $6p_{3/2}nf$ $[k=9/2]$, $6p_{3/2}nf$ $[k=5/2]$, and $6p_{3/2}nf$ $[k=7/2]$. The direct quadrupole term yields no splitting between $6p_{1/2}nf$ states.

The tentative assignment based upon oscillator strengths and fine-structure splittings in jk coupling was used as a starting point for MQDT analyses of all spectral data corresponding to a specific J value. In a previous paper [4] the details of the "phase-shifted reaction matrix" MQDT formalism were discussed and references given. This formalism is applied to calculate oscillator strength distributions dS/dE for a particular combination of relevant parameters (a set of quantum defects δ_i, dipole moments D_i, and reaction-matrix elements R'_{ij}) for the $6pnf$ channels involved. The calculated dS/dE distribution could be compared directly with the intensities in the observed spectra. After an initial optimization on the basis of trial and error the MQDT parameters were determined in a minimization routine. Uncertainties in the parameters could be deduced from the covariance matrix of the minimization procedure. To restrict the number of variables the reaction-matrix elements were taken to be independent of energy, interactions between channels corresponding to a common ionization limit were ignored, and continuum-continuum interactions neglected. Most importantly, for consistency spectra recorded using different excitation paths to the same final $6pnf$, J states were analyzed using a common set of parameters except for the dipole moments. The latter procedure was, e.g., followed to unravel the structure of $J=3$.

For simplicity each autoionizing series was treated as a bound channel with one continuum attached to it, which is assumed not to interact with the other bound channels. In the energy range of the $6pnf$ series no distinction has to be made between $6s\epsilon l$ and $5d\epsilon l$ continuum channels. So in the case of $J=4$ the three continua used in the analysis may represent one of the two possible even parity $J=4$ continuum channels ($6s_{1/2}\epsilon g_{7/2}$ or $6s_{1/2}\epsilon g_{9/2}$) or one of the ten possible $5d\epsilon l$ $J=4$ even-parity channels.

As a by product of this study between the broad, autoionizing $6pnf$ resonances, several weaker and much narrower members of $6pnp$ series were observed. The $5d6p$-$6pnp$ transitions are allowed in one-photon excitation, and by inspection of the angular-momentum part of the transition dipole matrix elements it follows that for these $\Delta l=-1$ transitions the $\Delta J=-1$ branch is dominant. These $6pnp$ states will be treated in Sec. III F.

A. $6pnf$ $J=5$

The $6p_{3/2}nf$ $J=5$ series was excited from the $5d6p\ ^3F_4$ intermediate state. For $J=5$ there is only a single $6pnf$ series converging to the upper $6p_{3/2}$ limit at 63 987.324 cm^{-1}. From the oscillator strength calculations assuming jk wave functions, it follows that the intensity of the $5d6p\ ^3F_4$–$6pnf$ $J=4$ transitions is an order of magnitude weaker. Therefore the spectrum, given in Fig. 2, and showing a regular unperturbed Rydberg series for $n=14$–57 is analyzed as a single progression. The

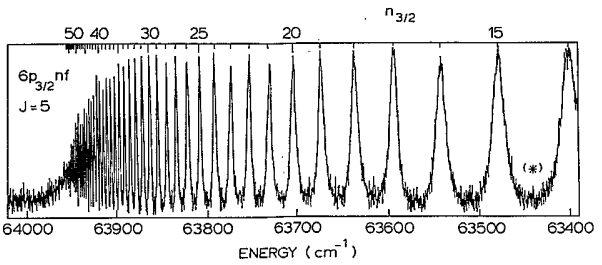

FIG. 2. Spectrum of the $6p_{3/2}nf$ $J=5$ autoionizing series as recorded in the excitation from the $5d6p\ ^3F_4$ intermediate state as a function of the wavelength of the second uv laser. The line marked with (*) is the $6p18p$ $J=3$ resonance.

relevant parameters resulting from a simple two-channel MQDT analysis are the quantum defect $\delta=0.30\pm0.01$ and the interaction matrix element between bound $6pnf$ series and continuum $R'_{1,\mathrm{cont}}=0.69\pm0.04$.

Apart from the $n=14$–57 members of the $6p_{3/2}nf$ Rydberg series also the $6p_{3/2}8f$ and $6p_{3/2}7f$ $J=5$ lines below the $6p_{1/2}$-ion limit were carefully recorded. From a fitting of the latter line shapes again the $R'_{1,\mathrm{cont}}$ element of the reaction matrix was determined: $R'_{1,\mathrm{cont}}=0.66\pm0.08$. No spectral features related to Rydberg series converging to the $6p_{1/2}$ limit were observed in excitation from the $5d6p\ ^3F_4$ intermediate state. This is consistent with the oscillator strength calculations for $5d6p\ ^3F_4$–$6p_{1/2}nf$ $J=3,4$ transitions (see Table I).

B. $6pnf$ $J=4$

The $6pnf$ $J=4$ series were observed in excitation from the $5d6p\ ^3F_3$ as well as from the $5d6p\ ^3D_3$ state. In Fig. 3 three parts of the extended spectrum excited from $5d6p\ ^3F_3$ (same intensity scale) are shown. The series converging to the $6p_{3/2}$ limit was observed for $n=10$–50, while the $6p_{1/2}nf$ series, observed for $n=15$–47, partly overlapped the broad $6p_{3/2}8f$ resonance.

The coupling of a p and an f electron results in two $6p_{3/2}nf$ and one $6p_{1/2}nf$ $J=4$ states. The calculation of oscillator strengths in jk-coupled wave functions shows that in excitation from the $5d6p\ ^3F_3$ intermediate state the $6p_{1/2}nf$ $J=2$ and 3 channels are a factor of 20 weaker than the $6p_{1/2}nf$ $J=4$ series. The $6p_{1/2}nf$ series in the lower part of Fig. 3 can therefore be unambiguously assigned as a single series converging to the $6p_{1/2}$ limit, possibly interacting with the $n=8$ member of the $6p_{3/2}nf$ series. The lower n members ($n=10$–15) of the $6p_{3/2}nf$ series clearly show asymmetric line shapes, indicating that more than one series is contributing to the signal intensity. The strongest signal appears at the low-energy side of each resonance, corresponding to a high quantum defect of about 0.31. This series is referred to as channel 1.

From a calculation of the energy level ordering according to Eq. (1) in the jk-coupling case it follows that the series $6p_{3/2}nf$ $[k=7/2]$ $J=4$ has the lowest-energy position. The series with the lower oscillator strength (as-

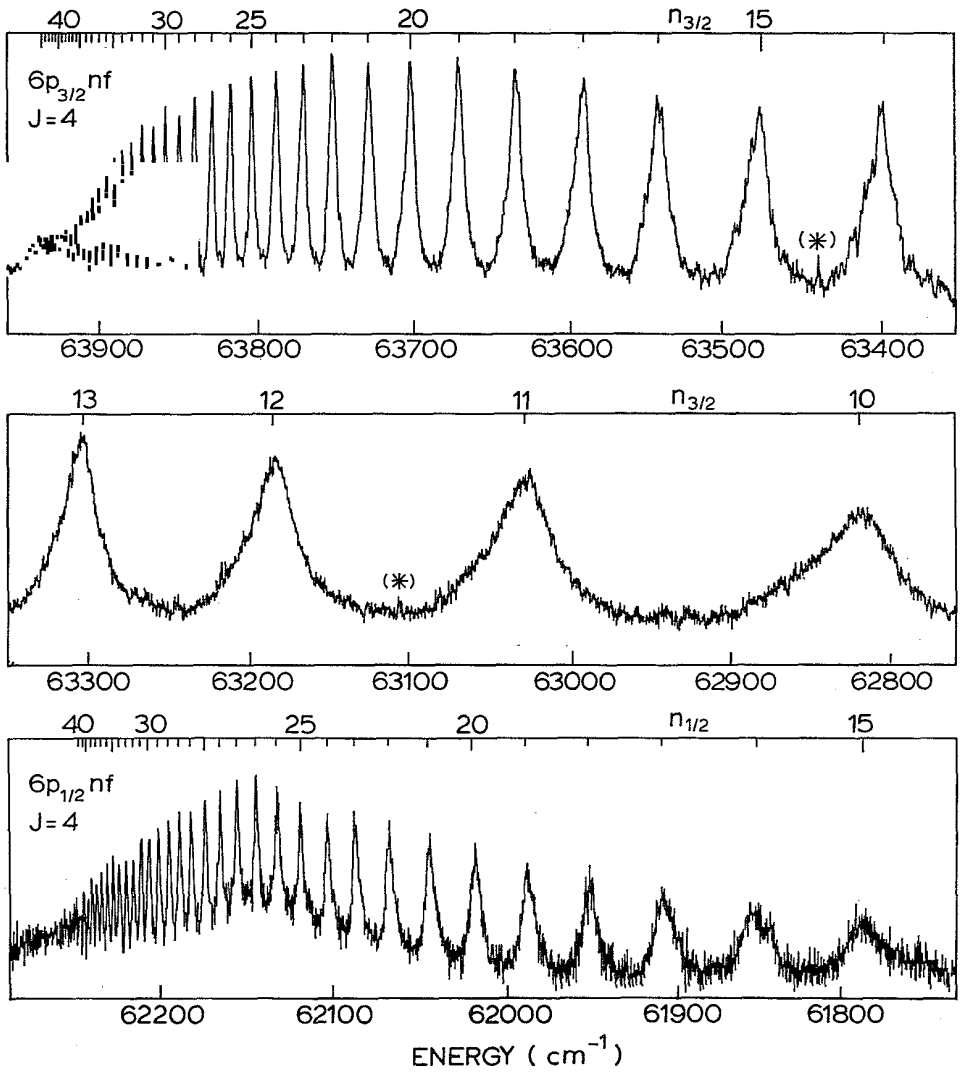

FIG. 3. Spectrum of the three interacting $6p_{3/2}nf\,J=4$ series as recorded in the excitation from the $5d6p\,^3F_3$ state. The $n_{3/2}$ scale marks the energy positions of members of the strong $6p_{3/2}nf\,[k=9/2]\,J=4$ series. The $6p_{3/2}nf\,[k=7/2]\,J=4$ states show as asymmetries on the left-hand side of the broad resonances, clearly visible for $n=10$–12. Note that the $6p_{1/2}nf$ series in the lower part interacts with the $6p_{3/2}8f$ states. Lines marked with (*) refer to $6pnp\,J=2$ states.

signed as channel 2) has an estimated quantum defect of about 0.16, while in the analysis of Sec. III C it is shown that the two $6p_{3/2}nf\,J=3$ series have quantum defects of 0.32 and 0.22, respectively. The preliminary fine-structure calculation places the $6p_{3/2}nf\,[k=9/2]\,J=4$ state higher in energy than the two $J=3$ states. Therefore channel 2 is tentatively assigned to have $J=4$. However, on the basis of a calculation of oscillator strengths for $5d6p\,^3F_3-6p_{3/2}nf$, J transitions the channel, denoted as $6p_{3/2}nf\,[k=9/2]\,J=4$ in jk coupling, is expected to give the strongest signal. From the energy level ordering in jk coupling and from the relative line intensities observed it appears that the other k component, the $6p_{3/2}nf\,[k=7/2]\,J=4$ state is dominant. This inconsistency will be addressed after completion of the analysis of the full multiplet in Sec. IV.

A spectrum of the $5d6p\,^3D_3-6p_{3/2}nf\,J$ transition was recorded for $n=18$–23. Again a pronounced Rydberg series with a quantum defect of $\delta=0.31$ appears as the dominant feature in the spectrum. This series coincides with channel 1 or the $6p_{3/2}nf\,[k=7/2]\,J=4$ series also observed in excitation from $5d6p\,^3F_3$. The oscillator strength calculation shows that in excitation from $5d6p\,^3D_3$ the $6p_{3/2}nf\,[k=7/2]\,J=4$ component is expected to be strongest. In this scheme the observed and calculated intensities are in agreement. A second series was visible as an asymmetry at the high-energy side of the main series. By deconvoluting the spectral lines in a double-peak analysis a quantum defect of $\delta=0.23\pm0.02$ was found for the minor feature. From the intensity calculation based upon jk wave functions it follows that this minor component has to be assigned, not as the second $[k,J=4]$ component, but as the $6p_{3/2}nf\,[k=5/2]\,J=3$ series.

TABLE II. MQDT parameters for the $6pnf\ J=4$ series in a six-channel model. The index i denotes the channel, I_i the ionization limit, and δ_i the quantum defect.

	1	2	3	4	5	6
i	$6p_{3/2}nf\ 4[k=7/2]$	$6p_{3/2}nf\ [k=9/2]$	$6p_{1/2}nf$	Continuum 1	Continuum 2	Continuum 3
I_i	63 987.32	63 987.32	62 296.24	42 034.90	42 034.90	42 034.90
δ_i	0.31(1)	0.16(4)	0.19(2)			

R' matrix

	1	2	3	4	5	6
1						
2	0.0					
3	0.0(1)	−0.31(4)				
4	0.61(3)	0.0	0.0			
5	0.0	0.82(8)	0.0	0.0		
6	0.0	0.0	0.60(3)	0.0	0.0	

The spectra, observed in the excitation from the $5d6p\ ^3F_3$ state, were analyzed in the framework of the phase-shifted formalism of MQDT, considering four channels above the $6p_{1/2}$ limit: two $J=4$ bound series converging to the $6p_{3/2}$ limit, each interacting with a continuum. The results from the minimization routine are collected in Table II (channels 1, 2, 4, and 5). The spectrum shown in the lower part of Fig. 3 was treated separately in a fitting routine. The parameters for the $6p_{3/2}nf$ series, as determined from the spectrum above the $6p_{1/2}$ limit, were kept constant, while channels 3 and 6 were added, representing the $6p_{1/2}nf$ series and an interacting continuum. The relative dipole moments for the $[k=9/2]$ and $[k=7/2]$ components were not taken from the calculations presented in Table I, but were adjusted to fit the observed spectrum. Parameters representing channel mixing between $6p_{3/2}nf$ and $6p_{1/2}nf$ series were also included. The resulting errors in the parameters for channel 2 are largest because of its weak excitation and the overlap with the stronger resonances of channel 1. From the MQDT analysis it follows that the $6p_{1/2}nf\ J=4$ series (channel 3) only significantly interacts with channel 2: the $6p_{3/2}nf\ [k=9/2]\ J=4$ series. As only one $6p_{3/2}nf$ resonance ($n=8$) was observed below the $6p_{1/2}$ limit superimposed on a large series of $6p_{1/2}nf$ lines, the spectral information did not allow for an investigation of differences in interaction matrix elements $R'_{i,\mathrm{cont}}$ (for $i=1,2$) above and below the $6p_{1/2}$ limit. The $6pnf\ J=4$ spectrum could be reproduced reasonably well in a calculation of the oscillator strength distribution dS/dE on the basis of R' parameters for the $6p_{3/2}nf$ and $6p_{1/2}nf$ series. As in the $5d6p\ ^3D_3$–$6p_{3/2}nf\ J$ spectrum two different noninteracting J series were excited, no attempt to perform a MQDT analysis was undertaken.

C. $6pnf\ J=3$

The case of $J=3$ is the most complicated in the $6pnf$ configuration because of the presence of four interacting series, two converging to each $6p_{1/2}$ and $6p_{3/2}$ ionization limit. For this reason these series were excited from different intermediate $5d6p\ J=2$ states. The $6p_{3/2}nf$ $J=3$ lines above the $6p_{1/2}$ limit were investigated in $5d6p\ ^1D_2$–$6pnf$ and $5d6p\ ^3D_2$–$6pnf$ transitions. A small part ($n=20$–22) of the spectra excited from $^1D_2$ and $^3D_2$ intermediate states is reproduced in Fig. 4. The resonances in the upper part of the spectrum, representing transitions from $5d6p\ ^1D_2$, are clearly narrower than

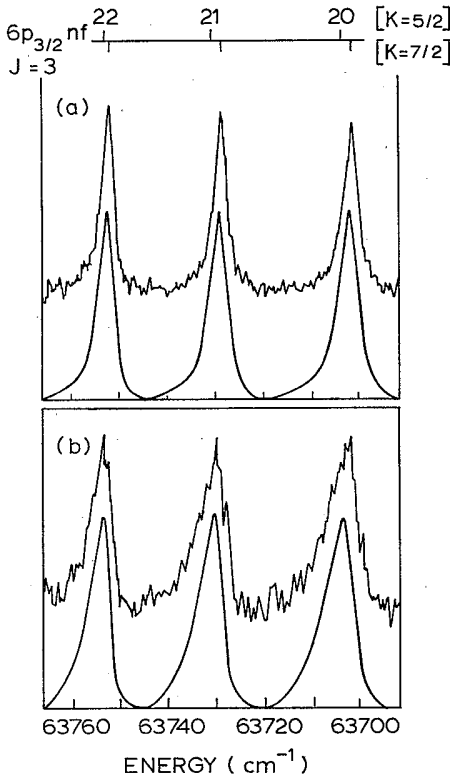

FIG. 4. Fraction of $6p_{3/2}nf\ J=3$ spectrum for $n=20$–22. Underneath the observed features a calculated spectrum is shown, using two noninteracting channels converging to the $6p_{3/2}$ limit with MQDT parameters of Table III and dipole moment parameters as discussed in Sec. III C. (a) Excitation from $5d6p\ ^1D_2$ and (b) excitation from $5d6p\ ^3D_2$.

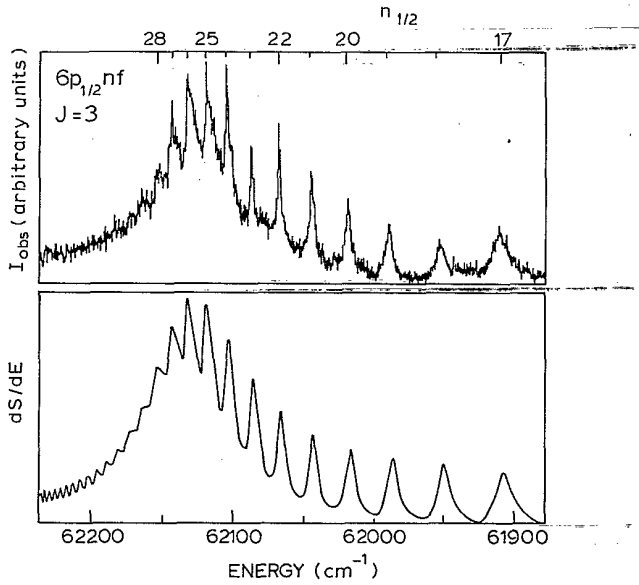

FIG. 5. Spectrum of the $6p_{1/2}nf\ J=3$ series interacting with the broad $6p_{3/2}8f\ J=3$ perturber recorded in excitation from the $5d6p\ ^1D_2$ intermediate state. The lower smooth curve represents the calculated oscillator strength distribution dS/dE calculated with the MQDT parameters of Table III.

those excited from $5d6p\ ^3D_2$, shown in the lower part of Fig. 4. Above the $6p_{1/2}$ limit the two autoionizing series are $6p_{3/2}nf\ [k=5/2]\ J=3$ and $6p_{3/2}nf\ [k=7/2]\ J=3$ in jk coupling. The calculated fine-structure splittings on the basis of jk coupling [Eq. (1)] show that both $J=3$ levels have a relatively large quantum defect, that the splitting between $J=3$ states is smaller than between $6p_{3/2}nf$ $J=4$ states, and that the $[k=7/2]\ J=3$ state has the largest quantum defect of the two $J=3$ series. Calculations of oscillator strengths, also in jk coupling, yield that both $6pnf\ J=3$ lines have equal intensity in excitation from the $5d6p\ ^3D_2$ state, while for excitation from the $^1D_2$ state an oscillator strength ratio of 4:1 is expected in favor of $[k=7/2]\ J=3$. These considerations are consistent with the observed spectra and the quantum defects derived. The excitation of two equally strong (in jk coupling) channels thus already explains qualitatively the larger width observed in the $5d6p\ ^3D_2-6pnf\ J=3$ resonances.

For a more quantitative analysis the oscillator strength distribution dS/dE was calculated in a MQDT-fitting routine, in which the dipole moments were fixed at the ratios predicted for jk coupling. Quantum defects as well as the R'-matrix coupling coefficients of both channels to a continuum were varied. The optimized oscillator strength distribution dS/dE, also shown in Fig. 4, was found for the following parameters: quantum defects $\delta_1=0.34\pm0.01$ and $\delta_2=0.23\pm0.05$ and MQDT reaction matrix elements $R'_{1,\mathrm{cont}}=0.49\pm0.02$ and $R'_{2,\mathrm{const}}=-0.79\pm0.08$. Channel 1 and 2 denote $6p_{3/2}nf\ [k=7/2]\ J=3$ and $6p_{3/2}nf\ [k=5/2]\ J=3$, respectively. The accuracy in channel 1 parameters is high as these can be extracted from an almost pure one-channel spectrum [Fig. 4(a)], while the information on channel 2 needs to be deconvoluted from overlapping resonances leading to larger errors. The $6p_{3/2}nf\ [k=5/2]\ J=3$ series appeared also in the $5d6p\ ^3D_3-6pnf$ spectrum as a minority constituent with the same quantum defect $\delta=0.23$.

Spectra of $6p_{1/2}nf\ J=3$ states were observed in excitation from three different intermediate states: $5d6p\ ^3D_2$, $5d6p\ ^1D_2$, and $5d6p\ ^3F_2$. A portion of the $5d6p\ ^1D_2-6p_{1/2}nf\ J=3$ spectrum for n ranging from 17 up to 28 is shown in Fig. 5. These states lie in the same energy range as both $6p_{3/2}8f\ J=3$ resonances, and the interference pattern of Fig. 5 as well as the strong n dependence of the quantum defects clearly indicate interaction. As no obvious splitting was observed, neither in the excitation from $^1D_2$ nor from $^3D_2$, both spectra were analyzed in terms of a single Rydberg series converging to the $6p_{1/2}$ ionization limit. Calculations of oscillator strengths, assuming jk-coupled wave functions for the $6p_{1/2}nf$ states, show that in transitions from the $5d6p\ ^1D_2$ intermediate state only the $6p_{1/2}nf\ [k=5/2]$ $J=3$ series is excited. For excitation from the $5d6p\ ^3D_2$ state an intensity ratio of 3:2 is expected between $6p_{1/2}nf$ $[k=5/2]\ J=3$ and $6p_{1/2}nf\ [k=7/2]\ J=3$ series, respectively. The observed spectra in both excitation

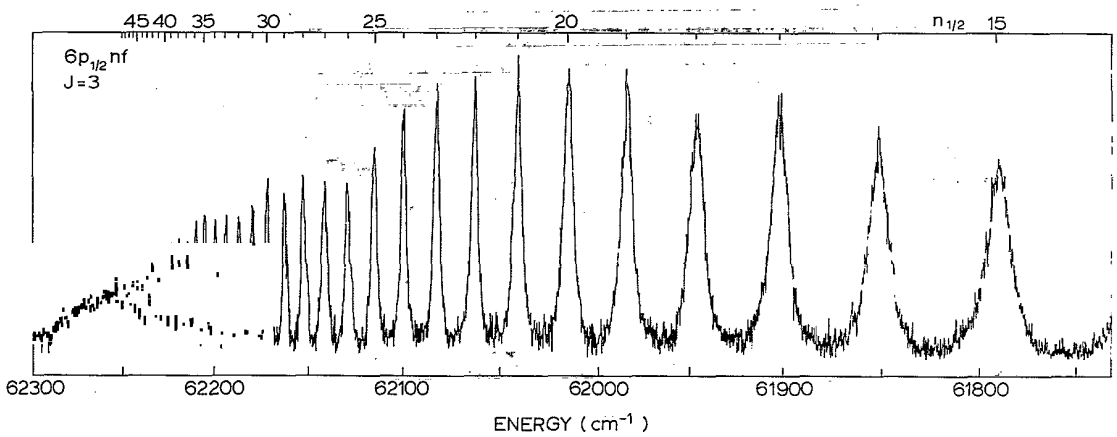

FIG. 6. Spectrum of the $6p_{1/2}nf\ J=3$ series excited from the $5d6p\ ^3F_2$ intermediate state. From the analysis in terms of line strengths it follows that the $6p_{1/2}nf\ [k=7/2]\ J=3$ series is excited.

schemes, however, do not give any indication for excitation of two $6p_{1/2}nf\,J=3$ series with a different quantum defect.

Outside the energy range of strong interaction the quantum defect of the $6p_{1/2}nf\,J=3$ series (denoted as channel 3) is $\delta_3=0.21\pm0.01$. Using fixed quantum defects and $R'_{i,\mathrm{cont}}$ matrix elements for the $6p_{3/2}nf\,J=3$ series a phase-shifted R'-matrix MQDT spectrum was constructed in a six-channel problem (three bound channels each interacting with a continuum) with the parameters of Table III. The dipole moments of the $6p_{3/2}nf$ $J=3$ series (channels 1 and 2) were fixed to the values obtained from the fitting routines of the spectra above the $6p_{1/2}$ limit. For the quantum defect of channel 3 the unperturbed value of $\delta=0.21$ was taken. Both spectra, from $5d6p\,^3D_2$ and $^1D_2$, were used in a minimization routine, and the fitting procedure was performed with only one set of quantum defects and R'-matrix parameters. A calculated spectrum using the parameters of Table III, for excitation from $5d6p\,^1D_2$ is included in Fig. 5, below the experimental spectrum. The overall structure is well reproduced by the calculations. $6p_{1/2}nf$ ($n>28$) lines show on the high-energy shoulder of the $6p_{3/2}8f$ resonance in the calculated oscillator strength distribution, but disappear in the noise in the observed spectrum. A similar comparison was made between observed and calculated $5d6p\,^3D_2$–$6p_{1/2}nf\,J=3$ spectra, again resulting in overall agreement.

A spectrum of the $6p_{1/2}nf\,J=3$ series excited from $5d6p\,^3F_2$ is reproduced in Fig. 6. It shows a strong Rydberg series converging to the $6p_{1/2}$ limit, without underlying effects of the $n=7$ and 8 members of $6p_{3/2}nf$ series. Calculated oscillator strengths for transitions from $5d6p\,^3F_2$ are in agreement with the nonappearance of any $6p_{3/2}nf\,J$ feature. Calculated intensities of the $5d6p\,^3F_2$–$6p_{3/2}nf\,J$ transitions are a factor of 20 weaker than the dominant series $6p_{1/2}nf\,[k=7/2]\,J=3$. Also calculated intensities of other $6p_{1/2}nf\,J$ components are low, and it is therefore justified to treat the spectrum as a single Rydberg series. The quantum defect of this $6p_{1/2}nf\,[k=7/2]\,J=3$ series, not observed in excitation from the other intermediate states $^1D_2$ and $^3D_2$, is found to be $\delta=0.31\pm0.01$. No perturbations in the quantum defects of the $6p_{1/2}nf\,[k=7/2]\,J=3$ levels were visible in the energy range of $6p_{3/2}nf$ states indicating that channel interaction is negligible. Therefore a simple two-channel MQDT analysis was performed for a determination of the continuum-interaction parameter: $R'_{i,\mathrm{cont}}=0.58\pm0.01$. This value is included in Table III.

D. $6pnf\,J=2$

The case of $J=2$ is similar to that of $J=4$ with two series converging to the $6p_{3/2}$ limit and one more to the $6p_{1/2}$ limit. Using $5d6p\,^3D_1$ as an intermediate state a spectrum was recorded in the energy range above and below the $6p_{1/2}$ limit. Broad $6p_{3/2}nf\,J=2$ resonances were recorded at poorer signal-to-noise ratio than in other spectra shown before. As an example, part of the $6p_{3/2}nf\,J=2$ spectrum is shown in Fig. 7 for $n=22$–26.

Calculations of oscillator strengths for $5d6p\,^3D_1$–$6pnf$ transitions in the approximation of jk-coupled $6pnf$ wave functions predict $6p_{3/2}nf\,[k=5/2]\,J=2$ to have by far the strongest intensity. The $6p_{3/2}nf\,[k=3/2]\,J=2$ series is expected to be extremely weak in excitation from $5d6p\,^3D_1$. The $5d6p\,^3D_1$–$6pnf\,J=1$ transition is, however, expected to appear in the spectrum at one third of the intensity of the main $6p_{3/2}nf\,[k=5/2]\,J=2$ component. The observed spectrum does not show any clear asymmetries, does not permit an analysis in terms of two

TABLE III. MQDT parameters for the $6pnf\,J=3$ series. The index i denotes the channel, I_i the ionization limit, and δ_i the quantum defect. The parameters for the first three channels and corresponding continua c_1, c_2, and c_3 were determined from a six-channel analysis of spectra obtained in excitation from $5d6p\,^1D_2$ and $^3D_2$. The parameters of channel 4, interacting with continuum c_4 were determined in an independent analysis of spectra excited from $5d6p\,^3F_2$, where no interaction with $6p_{3/2}nf\,J=3$ was observed. (Values of k for each state are given in square brackets.)

	1	2	3	4	5	6	7	8
i	$6p_{3/2}nf\,[k=7/2]$	$6p_{3/2}nf\,[k=5/2]$	$6p_{1/2}nf\,[k=5/2]$	$6p_{1/2}nf\,[k=7/2]$	c_1	c_2	c_3	c_4
I_i	63 987.32	63 987.32	62 296.24	62 296.24				
δ_i	0.34(1)	0.23(5)	0.21(1)	0.31(1)				
			R' matrix					
	1	2	3	4	5	6		
1								
2	0.0							
3	−0.14(4)	0.36(4)						
4	0.0(1)	0.0(1)	0.0					
5	0.49(2)	0.0	0.0	0.0				
6	0.0	−0.79(8)	0.0	0.0	0.0			
7	0.0	0.0	0.64(2)	0.0	0.0	0.0		
8	0.0	0.0	0.0	0.58(1)	0.0	0.0	0.0	

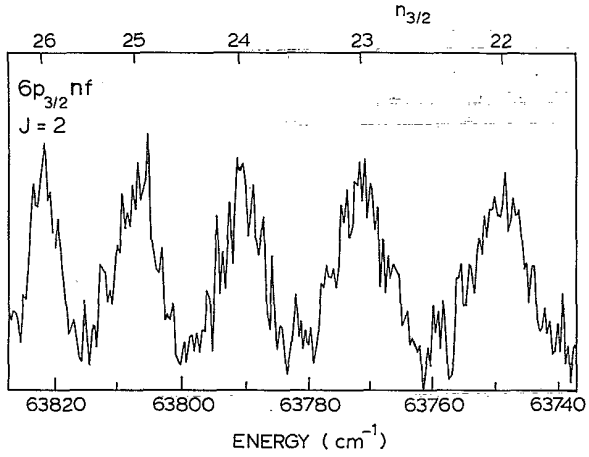

FIG. 7. Spectrum of $6p_{3/2}nf$ excited from the $5d6p\ ^3D_1$ intermediate state. From the analysis it follows that the series has to be assigned $6p_{3/2}nf$ $[k=5/2]$ $J=2$. Notice the large ratio $\Gamma/\Delta E$.

components contributing to lines as in the case of $J=4$, and was analyzed as a single series. The ratio between linewidth and energy spacing is $\Gamma/\Delta E=0.5$. In a simple MQDT analysis, using one bound and one continuum channel an averaged quantum defect of $\delta=0.21\pm0.02$ and a continuum interaction parameter $R'_{i,\mathrm{cont}}=1.00\pm0.15$ follow. The value for the quantum defect is close to that of the $6p_{3/2}nf$ $[k=5/2]$ $J=3$ series as expected in the limit of jk coupling. Direct information on the $6p_{3/2}nf$ $[k=3/2]$ $J=2$ series is lacking in the present investigation.

The spectrum below the $6p_{1/2}$ limit consists of a single $6p_{1/2}nf$ $J=2$ series interacting with $6p_{3/2}8f$ $J=2$ states. As the quantum defect of the second $6p_{3/2}nf$ $[k=3/2]$ $J=2$ series could not be derived from the spectrum above the $6p_{1/2}$ limit, no attempt was made to analyze channel mixing of the $6p_{1/2}nf$ and $6p_{3/2}nf$ series. To deduce an estimate for an averaged autoionization rate the phase-shifted MQDT formalism was used in the form of a simple two-channel analysis: a bound $6p_{1/2}nf$ series interacting with a single continuum. In the energy range of $n=16$–21 the effect of interaction with the $6p_{3/2}8f$ state is relatively small, even in the case of strong channel mixing, so that this procedure is allowed in first order. From this analysis, a quantum defect of $\delta=0.17\pm0.02$ and a continuum interaction parameter of $R'_{i,\mathrm{cont}}=0.60\pm0.03$ follow.

E. $6pnf$ $J=1$

Only one $6pnf$ $J=1$ series converging to the $6p_{3/2}$ limit exists. In a previous paper [4] details of the configuration interaction between the $6p_{3/2}nf$ and the four $6pnp$ $J=1$ series were analyzed. A spectrum of the $5d6p\ ^3P_0$–$6pnp,nf$ was presented in this previous paper. As will be discussed in Sec. V the influence of the interaction between $6pnp$ and $6pnf$ is not decisive for the overall structure of the broad $6pnf$ resonances. The quantum defect of $6pnf$ $J=1$ is $\delta_i=0.08\pm0.01$, while a value of $R'_{i,\mathrm{cont}}=0.66\pm0.04$ reproduces the overall widths of the long progression of autoionizing resonances above the $6p_{1/2}$ limit.

The $6p_{3/2}8f$ and $6p_{3/2}7f$ autoionizing resonances below the $6p_{1/2}$ limit are reproduced in calculations, involving the interactions with $6pnp$ $J=1$ states, on the basis of a reaction matrix element $R'_{i,\mathrm{cont}}=0.58\pm0.04$ for the interaction of $6pnf$ with a continuum. The phase-shifted R'-matrix parameters obtained for interactions of $6pnf$ $J=1$ states for $n=7$ and 8 with $6p_{1/2}np_{1/2}$ and $6p_{1/2}np_{3/2}$ channels are $R'=-0.20\pm0.05$ and $R'=-0.11\pm0.04$, respectively [4]. These parameters represent, in the energy range above the $6p_{1/2}$ limit, a coupling of the $6pnf$ states ($n>8$) to a $6p_{1/2}\epsilon p$ continuum.

F. $6pnp$ series

In between the relatively broad $6pnf$ resonances several much narrower but weak lines were observed in various spectra. In one-photon transitions from $5d6p$ intermediate states excitation of $6pnp$ states is expected with a dominating $\Delta J=-1$ branch. In three recent reports [4–6] the $6pnp$ $J=0$, 1, and 2 autoionizing series were analyzed in detail. In the present study several narrow resonances were observed, which could be assigned $6pnp$ $J=0$, 1, and 2 states. These will not be discussed here.

Information on the single $6p_{3/2}np_{3/2}$ $J=3$ series is scarce. Bente and Hogervorst [12] observed four $6p_{3/2}np$ resonances (for $n=11$, 12, 16, and 19) by making use of an isolated core excitation scheme $6snf$-$6pnp$. In this scheme the $6pnp$ $J=3$ states can only be excited through configuration interaction in the excited state with $6pnf$ $J=3$. Again, like in the case of $J=1$ [4], this was proof of $6pnp$-$6pnf$ configuration interaction. These states with a quantum defect of $\delta_p=3.81$ were tentatively assigned $J=2$ or 3. On the basis of reported values for the quantum defects for $J=2$ states [5] it was concluded that the $J=3$ Rydberg states were observed.

In the present observation of $5d6p\ ^3F_4$–$6pnp$ lines, appearing, e.g., in the spectrum of Fig. 2 and indicated with an asterisk, the $6pnp$ states can unambiguously be assigned $J=3$ because of one-photon selection rules. The positions and linewidths of observed $6pnp$ $J=3$ autoionizing states are listed in Table IV. The average quantum defect of $\delta_p=3.81$ agrees well with the value determined by Bente and Hogervorst [12], thus supporting their assignment. The widths of the observed resonances correspond to an averaged scaled autoionization width of $\Gamma(n^*)^3=0.018$ a.u. [full width at half maximum (FWHM)]. Recently the multiplet level structure for the $6pnp$ configuration was evaluated using a Slater-Condon analysis on the basis of nine out of ten observed series [6]. From their fine-structure constants for the $n=18$ manifold the energy position of $6p\,18p$ $J=3$ state was calculated to be 63442.3 cm^{-1}, close to the presently observed value of 63 441.8 cm^{-1} (Table IV).

TABLE IV. Observed energy positions (in cm^{-1}), linewidths Γ (in cm^{-1}) and quantum defects δ_p for $6p_{3/2}np_{3/2}$ $J=3$ autoionizing Rydberg states. The widths of lines marked with L are determined by the bandwidth of the uv laser (0.45 cm^{-1}).

State	Energy position	Γ_{obs}	δ_p
$6p_{3/2}13p_{3/2}$	62 685.9	4.7	3.817
$6p_{3/2}14p_{3/2}$	62 930.5	4.1	3.810
$6p_{3/2}18p_{3/2}$	63 441.8	0.5	3.817
$6p_{3/2}22p_{3/2}$	63 654.7	1.1	3.836
$6p_{3/2}24p_{3/2}$	63 718.2	L	3.808
$6p_{3/2}25p_{3/2}$	63 743.0	L	3.762
$6p_{3/2}26p_{3/2}$	63 765.4	L	3.805
$6p_{3/2}31p_{3/2}$	63 743.0	L	3.821

IV. ANALYSIS OF MULTIPLET STRUCTURE

In general, the energy levels within a two-electron configuration can be treated using the relevant multipole orders of the direct and exchange electrostatic interactions of both electrons represented by the well-known Slater integrals. The example of the fine structure of a pf configuration was discussed extensively by Cowan and Andrew [20], who included both electrostatic and spin-orbit effects. The splitting into 12 fine-structure states is governed by the $F^{(2)}$ direct and $G^{(2)}$ and $G^{(4)}$ exchange integrals of the electrostatic interaction and by the ζ_{6p} and ζ_{nf} spin-orbit interaction constants of the core and Rydberg electron. The standard definition and notations of Cowan [21] were adopted for the $F^{(k)}$ and $G^{(k)}$ expectation values of the multiplet expansion of the electrostatic energy. $F^{(0)}$ corresponds to the monopole term of the electrostatic interaction and is a constant for the multiplet. The energy of the center of gravity is determined by this $F^{(0)}$ term, minus a small correction which depends on the exchange parameters [21]. The value for the spin-orbit parameter of the core-electron will be close to that of the spin-orbit constant for the Ba^+ core, $\zeta_{6p}=1127.24$ cm^{-1} and is fixed at that value in the present analysis. The Slater integrals scale as n^{-3}. The fitting procedure for $F^{(k)}$, $G^{(k)}$, and ζ_{nf} parameters was not undertaken for each individual n value, but rather for a fictitious set of energy positions for $n=15$ derived from quantum defects. This eliminates the effects of channel perturbations from the multiplet structure analysis. These quantum defects, deduced from MQDT analyses, are averaged over whole Rydberg series resulting in improved accuracy of the Slater and Spin-orbit parameters. It should be noted that it is one of the characteristics of the phase-shifted R'-matrix MQDT formalism, that it yields the quantum defects of unperturbed channels.

The energy positions of the eleven observed multiplet components for $n=15$ were calculated from the quantum defects and are listed in Table V. The assignment of levels corresponding to states with a common J value was decided on the basis of calculated relative energy positions as discussed in Sec. III. The intensity calculation based upon jk-coupled wave functions for the $6p_{3/2}nf$ states were taken as a secondary criterion. In all cases the assignment based upon intensities supports the identification from the level ordering, except for the $5d6p\ ^3F_3$–$6p_{3/2}nf$ $J=4$ spectrum. Here the $6p_{3/2}nf$ $[k=7/2]$ $J=4$ series at the lowest-energy appears strongest in the observed spectrum, while its calculated line strength is much lower than for the $6p_{3/2}nf$ $[k=9/2]$ $J=4$ series. For the $6p_{1/2}nf$ states no splitting between k states is introduced by the direct term of the electrostatic interaction. Therefore the initial assignment had to be based solely upon the linestrength calculations.

The quantum defect of the $6p_{3/2}nf$ $[k=5/2]$ $J=3$ series was determined in the MQDT analysis of the spectrum excited from $5d6p\ ^3D_2$ with a rather low accuracy: $\delta=0.23\pm0.05$. From the fact that its value was found to reproduce exactly in an independent excitation from $5d6p\ ^3D_3$ it was considered to be justified to reduce this uncertainty in the input of the Slater-Condon analysis. The $6p_{3/2}nf$ $[k=9/2]$ $J=4$ series was observed only in

TABLE V. The level structure of the 12 $6p15f$ J multiplet states. In the second column quantum defects are given and in the third column energy positions derived from these quantum defects. In the fourth column calculated values from the fitting routines are given and in the fifth column deviations between calculated and observed values. All energy values are in cm^{-1}.

Multiplet component	Quantum defect	Energy position From quantum defects	Energy position Calc.	Obs.-Calc.
$6p_{3/2}nf$ $[k=9/2]$ $J=5$	0.30±0.01	63 479.5±0.7	63 480.1	−0.6
$6p_{3/2}nf$ $[k=7/2]$ $J=4$	0.31±0.01	63 478.8±0.7	63 479.3	−0.5
$6p_{3/2}nf$ $[k=9/2]$ $J=4$	0.13±0.02	63 491.0±1.4	63 492.5	−1.5
$6p_{1/2}nf$ $[k=7/2]$ $J=4$	0.19±0.02	61 796.1±1.4	61 795.1	+1.0
$6p_{3/2}nf$ $[k=7/2]$ $J=3$	0.34±0.01	63 476.7±0.7	63 476.0	+0.7
$6p_{3/2}nf$ $[k=5/2]$ $J=3$	0.23±0.02	63 484.3±1.4	63 484.5	−0.2
$6p_{1/2}nf$ $[k=5/2]$ $J=3$	0.21±0.01	61 794.8±0.7	61 795.1	−0.3
$6p_{1/2}nf$ $[k=7/2]$ $J=3$	0.31±0.01	61 787.9±0.7	61 787.9	0.0
$6p_{3/2}nf$ $[k=3/2]$ $J=2$			63 494.2	
$6p_{3/2}nf$ $[k=5/2]$ $J=2$	0.21±0.02	63 485.6±1.4	63 485.8	−0.2
$6p_{1/2}nf$ $[k=5/2]$ $J=2$	0.17±0.02	61 797.5±1.4	61 796.6	+0.9
$6p_{3/2}nf$ $[k=3/2]$ $J=1$	0.08±0.01	63 494.4±0.7	63 493.7	+0.7

one spectrum as a weak component resulting in a quantum defect $\delta=0.16\pm0.04$. In order to increase the accuracy in this value spectral data of Bente and Hogervorst obtained by isolated-core excitation were included in the MQDT analysis as well. This resulted in a quantum defect of $\delta=0.13\pm0.02$ for this series, which is consistent with the value already published [12] and confirmed independently by Jones *et al.* [14] (see also Sec. VI).

An analysis of the parameter space (see also [20]), that governs the multiplet structure of the pf configuration, reveals that three series are sensitive to a nonzero value of the $G^{(2)}$ exchange parameter: $6p_{3/2}nf$ $J=5$, $6p_{3/2}nf$ $[k=9/2]$ $J=4$, and $6p_{1/2}nf$ $[k=7/2]$ $J=3$. In Fig. 8 the effect of $G^{(2)}$ on the energy level structure of the $6p15f$ multiplet is graphically shown. On the left-hand side ($G^{(2)}=0$) the $6p_{3/2}nf$ states are split in four subsets of equidistant levels represented by their k values, while the $6p_{1/2}nf$ states all coincide. This situation where splittings are caused by the direct electrostatic interaction [equivalent to Eq. (1)] and the spin-orbit interaction of the core electron is the case of jk coupling ($G^{(2)}=G^{(4)}=\zeta_{nf}=0$), which was the starting point for the identification of levels in Sec. III.

In a least-squares minimization routine, in which the energy positions were weighted by their inverse accuracy, values for the Slater $F^{(0)}$, $F^{(2)}$, and $G^{(2)}$ parameters were obtained. For the diagonalization of the fine-structure energy matrix the coefficient matrix was taken from Cowan and Andrew [20]. It was found that the values for $G^{(4)}$ and ζ_{15f} are within the estimated error limits from the covariance matrix of the fitting routine. In a second run $G^{(4)}$ and ζ_{15f} were set to zero and the constants determined again. The results of the fit for the calculated energy positions as well as for the parameters are given in Tables V and VI, respectively. The value determined for the $F^{(0)}$ constant corresponds to a center of gravity energy of $62\,922.4\pm0.2$ cm^{-1} for the $6p15f$ multiplet.

The energy positions within the $6p15f$ manifold are well reproduced in the fitting routine, where each data point matches to the calculated value within the error limit. The experimental data points for the energies of $6p15f$ states, included in Fig. 8, also show the consistency of the model. Moreover the large effect of the Slater exchange integral $G^{(2)}$ manifests itself in the positioning of the $6p_{3/2}nf$ $J=5$ state and the lowest energy $6p_{1/2}nf$ $J=3$ state. From the resulting fine structure parameters the quantum defect of the one unobserved $6p_{3/2}nf$ $[k=3/2]$ $J=2$ series can be derived to be $\delta=0.08$.

The Slater-Condon multiplet analysis, in which an energy matrix is diagonalized, produces the composition of the $6pnf$ ($n=15$) wave functions. The mixing coefficients for the wave functions related to $J=2$, 3, and 4 states projected onto a $[j,k]$ basis are easily derived. The $6pnf$ $J=1$ and 5 are pure states. Configuration interactions with, e.g., $6pnp$ states, interactions with continuum states, and $6p_{1/2}nf$-$6p_{3/2}nf$ channel interaction, giving rise to additional mixing in the wave function composition are neglected. Under these assumptions the wave function composition of $6p_{3/2}nf$ J states on a $[j,k]$ basis is

J	ψ	$[j,k]$		$[j,k]$
4	$\psi_1=-0.38$	[3/2,9/2]	+0.92	[3/2,7/2]
	$\psi_2=0.92$	[3/2,9/2]	+0.38	[3/2,7/2]
3	$\psi_1=0.97$	[3/2,7/2]	+0.24	[3/2,5/2]
	$\psi_2=-0.24$	[3/2,7/2]	+0.97	[3/2,5/2]
2	$\psi_1=0.999$	[3/2,5/2]	−0.004	[3/2,3/2]
	$\psi_2=0.004$	[3/2,5/2]	+0.999	[3/2,3/2]

So up to 14% admixture of a second state into the wave function of the $[j,k]$ states is found. Mixing coefficients

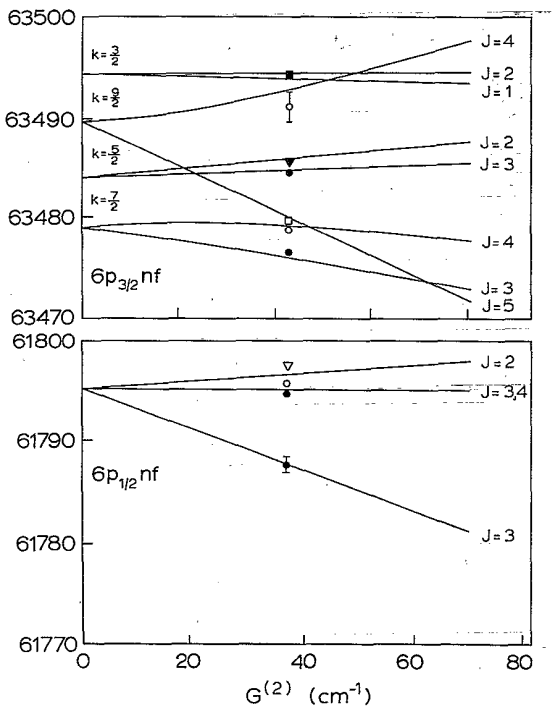

FIG. 8. Fine-structure splittings between $6p_{3/2}15f$ J states (upper part) and $6p_{1/2}15f$ J states (lower part) as a function of the $G^{(2)}$ exchange interaction parameter, with a center of gravity energy of 62 922.4 cm^{-1} and $F^{(2)}=52$ cm^{-1} taken to be constant. The experimental data points are plotted at the optimized value of $G^{(2)}$ as determined in the fit. Different symbols represent J values: (■) $J=1$, (▼) $J=2$, (●) $J=3$, (○) $J=4$, and (□) $J=5$. Experimental error (see Table V), either 0.7 or 1.4 cm^{-1}, are shown for two data points.

TABLE VI. Values (in cm^{-1}) for Slater $F^{(k)}$ and $G^{(k)}$ integrals representing the fine structure of the $6p15f$ multiplet. The values for $G^{(4)}$ and ζ_{15f} were set to zero. ζ_{6p} was set to the value for the spin-orbit constant of the ion: 1127.24 cm^{-1}.

$F^{(0)}$	501.3±0.2
$F^{(2)}$	52±3
$G^{(2)}$	37±2

for $6pnf$ on a jj-coupled basis were derived by applying a $jk \rightarrow jj$ basis transformation [20]. Especially the $J=4$ states are found to be largely mixed (34%).

Using the actual wave-function composition the line strengths of all relevant $5d6p$-$6pnf$ transitions were recalculated. Values are listed in the last column of Table I. Comparison of these values with the values calculated on a jk basis shows no drastic deviations, thus indicating that the tentative assignment based upon jk line strengths is a reliable one. More specifically the oscillator strength calculations with the actual wave functions are in better agreement with some striking characteristics of the observed spectra. In excitation from $5d6p\ ^3F_2$ and $^3F_4$ states indeed only a single series is observed, the $6p_{3/2}nf$ $J=5$ and the $6p_{1/2}nf$ $[k=7/2]$ $J=3$ series, respectively. The most important difference is found in the intensities for excitation from $5d6p\ ^3F_3$, where an inconsistency was left in the assignment of $6p_{3/2}nf$ $[k=7/2$ and $9/2]$ $J=4$ channels on the basis of level splittings and intensities. The intensities calculated from the actual $6pnf$ wave functions show that the $k=7/2$ series (with $\delta=0.31$) is most strongly excited, therewith removing the earlier inconsistency.

In principle, the oscillator strengths in transitions observed from different intermediate states may be compared with calculated values of Table I. As discussed in Sec. II the relative number density of atoms prepared in $5d6p$ states and uv laser power are constant in different excitations. However, as day-to-day variations in the total atomic beam density, spatial (laser) beam quality, and beam overlap could not be controlled completely, only tentative conclusions may be drawn from a comparison of observed intensities. The highest signal intensities, reflected in large signal-to-noise ratio, were found in the spectra of $5d6p\ ^3F_4$–$6p_{3/2}nf$ $J=5$ (Fig. 2), $5d6p\ ^3F_2$–$6p_{1/2}nf$ $J=3$ (Fig. 6), and $5d6p\ ^1D_2$–$6p_{3/2}nf$ $J=3$ [Fig. 4(a)], while the spectrum of $5d6p\ ^3D_1$–$6p_{3/2}nf$ $J=2$ [Fig. 4(a)] was found to be weak. These major characteristics agree well with the calculations.

Calculations of line strengths for transitions from $5d6p$ intermediate states other than the ones used in the present experiment show that the unobserved $6p_{3/2}nf$ $[k=3/2]$ $J=2$ series may be well observed from $5d6p\ ^3P_1$ in an almost pure spectrum. In excitation from the $5d6p\ ^1P_1$ state both $J=2$ series are expected to be equally strong.

V. AUTOIONIZATION PROBABILITIES

The reaction matrix elements $R'_{i,\mathrm{cont}}$, between a bound $6pnf$ channel and an open (continuum) channel, as determined from MQDT analyses, are a measure of the scaled autoionization width Γ (in atomic units), at full width half maximum (FWHM) through [15]:

$$\Gamma(n^*)^3=2(R'_{i,\mathrm{cont}})^2/\pi\ . \tag{2}$$

Here n^* is the effective principal quantum number of the state ($n^*=n-\delta$). Values for the autoionization widths Γ are derived from $R'_{i,\mathrm{cont}}$ parameters and compared with calculations of Poirier [17,18] for the widths of $6p24f$ states in Table VII. Instead of directly measured values of the autoionization widths of $6p24f$ states, we used $R'_{i,\mathrm{cont}}$ parameters deduced from analyses of complete series were used. This results in a better accuracy. Autoionization widths of $6p_{1/2}nf$ J states are n dependent, not only because of the n^{-3} scaling law, but also because of n-dependent mixing with $6p_{3/2}nf$ perturbers. Here also the widths of the $6p_{1/2}24f$ states as derived from the parameter denoting the direct coupling with the continuum were used. Note that in this procedure the widths of $6p_{1/2}24f,J$ states are underestimated by the neglect of the effect of the channel interaction with $6p_{3/2}nf$ states.

TABLE VII. Observed and calculated [18] autoionization widths Γ (FWHM) for $6p24f$ J resonances. The calculations relate to jk-coupled states and the k-quantum number is given. The observations relate to $R'_{i,\mathrm{cont}}$ parameters of the phase-shifted matrix elements, where a tentative k-quantum number is also given for comparison. Values in parentheses denote an error in the last digit. Widths are in atomic units, corresponding to 219 475 cm^{-1}.

	Γ Observed		Γ Calculated
$6p_{3/2}nf$ $J=5$	$2.3(3)\times10^{-5}$	$6p_{3/2}nf$ $[k=9/2]$	1.58×10^{-5}
$6p_{3/2}nf$ $[k=9/2]$ $J=4$	$3.2(6)\times10^{-5}$		
$6p_{3/2}nf$ $[k=7/2]$ $J=4$	$1.8(2)\times10^{-5}$	$6p_{3/2}nf$ $[k=7/2]$	1.00×10^{-5}
$6p_{3/2}nf$ $[k=7/2]$ $J=3$	$1.2(1)\times10^{-5}$		
$6p_{3/2}nf$ $[k=5/2]$, $J=3$	$3.0(6)\times10^{-5}$	$6p_{3/2}nf$ $[k=5/2]$	1.68×10^{-5}
$6p_{3/2}nf$ $[k=5/2]$ $J=2$	$4.7(14)\times10^{-5}$		
$6p_{3/2}nf$ $[k=3/2]$ $J=2$		$6p_{3/2}nf$ $[k=3/2]$	1.56×10^{-5}
$6p_{3/2}nf$ $J=1$	$2.0(2)\times10^{-5}$		
$6p_{1/2}nf$ $J=4$	$1.7(2)\times10^{-5}$	$6p_{1/2}nf$ $[k=7/2]$	1.37×10^{-5}
$6p_{1/2}nf$ $[k=7/2]$ $J=3$	$1.6(1)\times10^{-5}$		
$6p_{1/2}nf$ $[k=5/2]$ $J=3$	$1.8(2)\times10^{-5}$	$6p_{1/2}nf$ $[k=5/2]$	1.08×10^{-5}
$6p_{1/2}nf$ $J=2$	$1.7(2)\times10^{-5}$		

The calculations of Poirier [17,18] for $6p24f$ were based upon the assumption that a long-range direct electrostatic interaction between core and Rydberg electron is responsible for the autoionization. Autoionization was considered into $6s\epsilon l$ and $5d\epsilon l$ [17] and $6p_{1/2}\epsilon l$ continuum channels [18]. The effects of electron spin of the outer electron and exchange contributions to the autoionization amplitude were ignored, and the rates are given for jk-coupled states.

The values obtained for the autoionization width in Table VII all fall in the range $0.8-3\times10^{-5}$ a.u. The calculations of Poirier predict widths that either agree well or are up to a factor of 2 narrower, dependent on the k state. Even for the case of the $6pnf$ $J=5$ states [11], where the assumption of a pure Coulombic direct interaction is better, a deviation between calculation and observation of a factor of 2 was found. Also for that case observations gave larger values. The widths of $6pnd$ states [7] could not be reproduced in this model, as the observed autoionization widths are an order of magnitude narrower than the predictions. Deviations are even more pronounced for $6pnp$ states [4]. In view of all these facts the intermediate case of $l=3$ for the Rydberg electron is remarkably well described by the model of long-range Coulombic forces as being responsible for autoionization. Apparently in the case of a $6p$ ionic core short-range effect, core overlap and exchange contribution do not play a significant role for the autoionization of $l=3$ electrons.

Inspection of the autoionization rates for the different $6p_jnf$ $[k]$ J fine-structure states show an overall agreement between the Γ derived from MQDT analyses and the values calculated with Poiriers model. First of all it appears that the grouping (in Table VII) of Γ according to jk values has significance. The observed autoionization rates for $6p_{1/2,3/2}nf$ $[k=5/2]$ and $6p_{3/2}nf$ $[k=9/2]$ states are indeed the largest as predicted. The Γ values for the $6p_{3/2}nf$ $[k=5/2]$ subgroup are highest both in observation and in calculation, although there is a discrepancy of a factor of 2 in the absolute numbers.

Although only autoionization into $5d\epsilon l$ and $6s\epsilon l$ channels was observed in the experiments, some information on autoionization into $6p_{1/2}\epsilon l$ channels could be deduced. The autoionization width of $6p_{3/2}nf$ $J=1$ states above the $6p_{1/2}$ limit is found to be 25% larger than for the $6p_{3/2}nf$ ($n=7$ and 8) $J=1$ states below this limit. However, from the coupling constants between $6p_{3/2}nf$ $J=1$ (for $n=7$ and 8) and $6p_{1/2}np_{1/2,3/2}$ $J=1$ series [4] a branching ratio of 15% is found for $6p_{3/2}nf$ autoionizing into $6p_{1/2}\epsilon p$ $J=1$ continua. For $J=1$ the $6p_{1/2}\epsilon p$ continua are the only open $6p_{1/2}\epsilon l$ even parity channels. The deviation between the value of 25% deduced from a reduction of the width of the broad $n=7$ and 8 resonances and the value of 15% deduced from channel mixing is not too large in view of the limited accuracy in the determination of these values. For the $6p_{3/2}nf$ $J=5$ series the situation is different, as autoionization into $6p_{1/2}\epsilon h$ is the only possibility. In the experiment the autoionization widths of $6pnf$ $J=5$ above and below the $6p_{1/2}$ limit are found to be equal, indicating that configuration interaction between $6pnf$ and $6pnh$ is not large. The spectra of $6p_{3/2}nf$ $J=2$, 3, and 4, each containing two series, did not allow for an inspection of differences between widths above and below the $6p_{1/2}$ limit. However, the channel mixing parameters between $6p_{3/2}nf$ and $6p_{1/2}nf$ series as obtained in the MQDT analyses below the $6p_{1/2}$ limit represent also $6p_{3/2}nf$-$6p_{1/2}\epsilon f$ interaction above the $6p_{1/2}$ limit. From a comparison of R'-matrix elements for $6p_{3/2}nf$ series interacting directly with $5d\epsilon l$ or $6s\epsilon l$ continua (through $R'_{i,\mathrm{cont}}$ for $i=1,2$) as well as with the $6p_{1/2}\epsilon f$ continuum (through $R'_{i,3}$ for $i=1,2$) branching ratios for $J=3$ and series could be derived. From the data of Tables III and IV the following branching ratios for autoionization into $6p_{1/2}\epsilon f$ were obtained:

State	Branching ratio (%)
$6p_{3/2}nf$ $[k=9/2]$ $J=4$	13
$6p_{3/2}nf$ $[k=7/2]$ $J=4$	<3
$6p_{3/2}nf$ $[k=7/2]$ $J=3$	8
$6p_{3/2}nf$ $[k=5/2]$ $J=3$	17

It should be noted that for $J=3$ as well as for $J=4$ autoionization into $6p_{1/2}\epsilon p$ and $6p_{1/2}\epsilon h$ is not possible, $6p_{1/2}\epsilon f$ being the only available $6p_{1/2}\epsilon l$ channel. So it can be concluded that autoionization into the $5d\epsilon l$ and $6s\epsilon l$ channels, producing the fast electrons detected in the present investigation, indeed was dominant. Therefore, the assignments based on calculated line strengths as used in Sec. III and IV are correct.

Some indication for relative autoionization into $5d\epsilon l$ $6s\epsilon l$ channels could be obtained. By varying the voltage on the repelling grid steep drops were observed in the total amount of electrons detected at the energy thresholds for electrons produced in $5d\epsilon l$ and $6s\epsilon l$ autoionization. From the thus obtained rather crude electron energy spectrum a ratio of 2:1 for autoionization into $5d\epsilon l$ versus $6s\epsilon l$ channels was found for the $6p_{3/2}nf$ $[k=7/2]$ $J=4$ series. The resolution of this method was too low to discriminate between $5d_{3/2}\epsilon l$ and $5d_{5/2}\epsilon l$ channels.

VI. DISCUSSION

A number of fine-structure states were observed in previous studies on $6pnf$ autoionizing series, making use of the isolated-core excitation mechanism. In the work of Bente and Hogervorst [12] the lack of detail in the $6p_{1/2}nf$ spectra prevented any J value assignment. Above the lower $6p_{1/2}$ limit two overlapping Rydberg series were observed; the stronger, with a quantum defect of $\delta_f=0.27-0.35$, was assigned $6p_{3/2}nf$ $[k=7/2]$ $J=3$ or 4. This series clearly corresponds to channel 1 of the $J=4$ manifold with a quantum defect $\delta_f=0.31\pm0.01$ in the present investigation. In a setup with three circularly polarized lasers Jones, Dai, and Gallagher [14] were able to resolve several $6pnf$ J states and $J=4$ was analyzed in detail. The data were treated in a six-channel MQDT analysis involving the three $6pnf$ $J=4$ series and three continua, similar as in the present work, without, howev-

er, neglecting interactions between different continua and between channels converging to a common limit. The three quantum defects for the series described in *jj* notation $\delta_1[6p_{3/2}nf_{5/2}\ J=4]=0.31$, $\delta_2[6p_{3/2}nf_{7/2}\ J=4]=0.13$, and $\delta_3[6p_{1/2}nf_{7/2}\ J=4]=0.20$ agree well with the presently observed values. The parameters for the direct interaction of the two $6p_{3/2}nf$ channels with the continua R'_{14} and R'_{25} also agree well, while the continuum interaction parameter for the $6p_{1/2}nf_{7/2}$ $J=4$ series in the present work is lower ($R'_{3,\mathrm{cont}}=0.60\pm0.03$ instead of $R'=0.87$). As no error analysis was performed on the parameters derived by Jones, Dai, and Gallagher [14], it is unclear whether this is a significant deviation.

The analysis of the multiplet structure is one of the first for a relatively large number of terms in an autoionizing configuration. An important outcome of the multiplet analysis in terms of Slater integrals is that a large value for the $G^{(2)}$ exchange parameter is obtained. Thus exchange effects are found to be important for a reproduction of the fine-structure level ordering in the $6pnf$ configuration. The value for the spin-orbit constant of the Rydberg electron was found not to deviate significantly from zero, indicating that a *jj*-coupling scheme is not appropriate.

In several recent studies no splittings of $6p_{1/2}nl$ states were observed, neither in $6p_{1/2}nd$ [9] and $6p_{1/2}ng$ [11] series, nor in the ICE studies of $6p_{1/2}nf$ [12]. From this fact it was concluded that exchange effects were not important for the multiplet structure of $6pnl$ states. However, in a recent comprehensive study the $6pnp$ configuration was analyzed based upon the observation of nine out of ten series. The present measurement of the energy position of the tenth $6pnp$ $J=3$ series turns out to be in agreement with the predicted value from this multiplet analysis [6]. In $6pnp$ the contributions of direct and exchange Slater integrals to the electrostatic energy were found to be of the same order of magnitude. From this point of view the results on $6pnp$ and $6pnf$ configurations are comparable. Both $6pnp$ and $6pnf$ configurations are represented best in a *jk*-coupling scheme.

Jones, Dai, and Gallagher suggest (in Table II of Ref. [14]), assuming near *jj* coupling in the $J=4$ $6pnf$ series, a correction of the singlet-triplet mixing coefficients of the $6snf\ ^1F_3, ^3F_3$ series as previously determined by Post, Vassen, and Hogervorst [22] from hyperfine structure measurements. In view of the large mixing of $J=4$ channels on a *jj* basis (34%), as determined in the present multiplet analysis, this seems unjustified.

In the present study the configuration interactions were restricted to channel mixing between $6p_{3/2}nf$ and $6p_{1/2}nf$. Effects of other possible even parity perturbers such as $6pnp$ and $6pnh$ were neglected as they would not significantly affect the spectral features of the broad $6pnf$ resonances. The example of the $6p_{1/2}nf$ $J=1$ series [4] showed indeed that there is considerable configuration interaction between $6pnp$ and $6pnf$ series, manifesting itself in broadening effects, in asymmetric Fano-profiles, and shifts in the energy positions of $6p_{1/2}np_{1/2}$ $J=1$ states. But in reverse this example showed that a manifold of narrow resonances does not affect line position or overall line shape of a broad perturber. Therefore it seems justified to ignore the effect of interactions of the extremely narrow $6pnp$ and $6pnh$ [12] resonances on the broad $6pnf$ features.

As a final comment we note that the $6pnf$ states autoionize extremely rapidly. The width of 3×10^{-5} a.u. for one of the $6p24f$ states corresponds to a lifetime of 0.8 ps. For comparison the roundtrip time for an oscillating wave packet in an orbit with $n=24$ is 2 ps. Of all $6pnl$ states the $l=3$ case gives the broadest resonances. The $6p_{3/2}nf$ $[k=5/2]$ $J=2$ series is found to autoionize most rapidly, with a linewidth Γ, which is half the energy spacing between subsequent n states.

ACKNOWLEDGMENTS

The authors wish to thank M. Poirier for making available the results of a calculation of autoionization rates in $6pnf$ states and for his permission to use them in the present work and M. Brilleslijper for his help in the calculation of oscillator strengths. They gratefully acknowledge financial support from the Foundation for Fundamental Research on Matter (FOM) and the Netherlands Organization for the Advancement of Research (NWO). One of us (M.A.) wishes to thank the Netherlands University Foundation for International Cooperation (NUFFIC) for support.

*On leave from Department of Physics, Cairo University, Giza, Egypt.

[1] W. R. S. Garton and W. H. Parkinson, Proc. R. Soc. London, Ser. A **341**, 45 (1974).
[2] C. M. Brown and M. L. Ginter, J. Opt. Soc. Am. **68**, 817 (1978).
[3] R. Kachru, N. H. Tran, P. Pillet, and T. F. Gallagher, Phys. Rev. A **31**, 218 (1985).
[4] R. J. de Graaff, W. Ubachs, W. Hogervorst, and M. Abutaleb, Phys. Rev. A **42**, 5473 (1990).
[5] J. G. Story, E. G. Yap, and T. F. Gallagher, Phys. Rev. A **39**, 5127 (1989).
[6] B. Carre, P. d'Oliveira, P. R. Fournier, F. Gounand, and M. Aymar, Phys. Rev. A **42**, 6545 (1990).
[7] S. A. Bhatti, C. L. Cromer, and W. E. Cooke, Phys. Rev. A **24**, 161 (1981).
[8] F. Gounand, T. F. Gallagher, W. Sandner, K. A. Safinya, and R. Kachru, Phys. Rev. A **27**, 1925 (1983).
[9] R. Kachru, H. B. van Linden van den Heuvel, and T. F. Gallagher, Phys. Rev. A **31**, 700 (1985).
[10] O. C. Mullins, Y. Zhu, H. B. van Linden van den Heuvel, and T. F. Gallagher, Phys. Rev. A **32**, 2234 (1985).
[11] S. M. Jaffe, R. Kachru, H. B. van Linden van den Heuvel, and T. F. Gallagher, Phys. Rev. A **32**, 1480 (1985).
[12] E. A. J. M. Bente and W. Hogervorst, J. Phys. B **23**, 1403 (1990).
[13] R. R. Jones and T. F. Gallagher, Phys. Rev. A **38**, 2846 (1988).

[14] R. R. Jones, C. J. Dai, and T. F. Gallagher, Phys. Rev. A **41**, 316 (1990).
[15] W. E. Cooke and C. L. Cromer, Phys. Rev. A **32**, 2725 (1985).
[16] S. I. Nikitin and V. N. Ostrovsky, J. Phys. B **13**, 1961 (1980).
[17] M. Poirier, Phys. Rev. A **38**, 3484 (1988).
[18] M. Poirier (private communication).
[19] P. Grundevik, H. Lundberg, L. Nilsson, and G. Olsson, Z. Phys. A **306**, 195 (1982).
[20] R. D. Cowan and K. L. Andrew, J. Opt. Soc. Am. **55**, 502 (1965).
[21] R. D. Cowan, *The Theory of Atomic Structure and Spectra* (University of California Press, Berkeley, 1981).
[22] B. H. Post, W. Vassen, and W. Hogervorst, J. Phys. B **19**, 511 (1986).